

## Water Resources Research

### RESEARCH ARTICLE

10.1002/2016WR020033

#### Special Section:

Responses to Environmental Change in Aquatic Mountain Ecosystems

#### Key Points:

- High-resolution energy-balance model is used to quantify future changes to the magnitude, timing, and source of coastal runoff
- Climate models predict a 12–21% increase in annual precipitation and 2.5–4.3°C increase in annual temperature across study domain
- Runoff increases by 9–14% from increased autumn and winter rainfall runoff; glacier runoff decreases by 14–34% from reduced glacier extent

#### Supporting Information:

- Supporting Information S1

#### Correspondence to:

J. P. Beamer,  
jordan.beamer@gmail.com

#### Citation:

Beamer, J. P., D. F. Hill, D. McGrath, A. Arendt, and C. Kienholz (2017), Hydrologic impacts of changes in climate and glacier extent in the Gulf of Alaska watershed, *Water Resour. Res.*, 53, 7502–7520, doi:10.1002/2016WR020033.

Received 28 OCT 2016

Accepted 14 JUL 2017

Accepted article online 20 JUL 2017

Published online 1 SEP 2017

## Hydrologic impacts of changes in climate and glacier extent in the Gulf of Alaska watershed

J. P. Beamer<sup>1,2</sup> , D. F. Hill<sup>3</sup>, D. McGrath<sup>4,5</sup> , A. Arendt<sup>6</sup> , and C. Kienholz<sup>7,8</sup> 

<sup>1</sup>Water Resources Engineering, Oregon State University, Corvallis, Oregon, USA, <sup>2</sup>Now at Oregon Water Resources Department, Salem, Oregon, USA, <sup>3</sup>School of Civil and Construction Engineering, Oregon State University, Corvallis, Oregon, USA, <sup>4</sup>Alaska Science Center, U.S. Geological Survey, Anchorage, Alaska, USA, <sup>5</sup>Geosciences Department, Colorado State University, Fort Collins, Colorado, USA, <sup>6</sup>Polar Science Center, Applied Physics Laboratory, University of Washington, Seattle, Washington, USA, <sup>7</sup>Geophysical Institute, University of Alaska Fairbanks, Fairbanks, Alaska, USA,

<sup>8</sup>Natural Sciences Research Lab, University of Alaska Southeast, Juneau, Alaska, USA

**Abstract** High-resolution regional-scale hydrologic models were used to quantify the response of late 21st century runoff from the Gulf of Alaska (GOA) watershed to changes in regional climate and glacier extent. NCEP Climate Forecast System Reanalysis data were combined with five Coupled Model Intercomparison Project Phase 5 general circulation models (GCMs) for two representative concentration pathway (RCP) scenarios (4.5 and 8.5) to develop meteorological forcing for the period 2070–2099. A hypsographic model was used to estimate future glacier extent given assumed equilibrium line altitude (ELA) increases of 200 and 400 m. GCM predictions show an increase in annual precipitation of 12% for RCP 4.5 and 21% for RCP 8.5, and an increase in annual temperature of 2.5°C for RCP 4.5 and 4.3°C for RCP 8.5, averaged across the GOA. Scenarios with perturbed climate and glaciers predict annual GOA-wide runoff to increase by 9% for RCP4.5/ELA200 case and 14% for the RCP8.5/ELA400 case. The glacier runoff decreased by 14% for RCP4.5/ELA200 and by 34% for the RCP8.5/ELA400 case. Intermodel variability in annual runoff was found to be approximately twice the variability in precipitation input. Additionally, there are significant changes in runoff partitioning and increases in snowpack runoff are dominated by increases in rain-on-snow events. We present results aggregated across the entire GOA and also for individual watersheds to illustrate the range in hydrologic regime changes and explore the sensitivities of these results by independently perturbing only climate forcings and only glacier cover.

### 1. Introduction

The biophysical influence of runoff generated from mountain regions extends from the immediate watershed to downstream environments. In the case of coastal mountain regions, runoff influences the nearshore marine environment through impacts on coastal currents [Royer and Grosch, 2006], biogeochemistry [Fellman et al., 2010], and ecology [Hickey and Banas, 2003; Reisdorph and Mathis, 2014]. There is a significant interest in understanding the present spatiotemporal distribution of runoff into the Gulf of Alaska (GOA; Figure 1) [Beamer et al., 2016; Hill et al., 2015; Neal et al., 2010] in order to make meaningful predictions of how that distribution may change in the future in response to changes in precipitation, temperature, and land cover. High-latitude coastal mountain environments such as the GOA watershed are characterized by short residence times, large annual fluxes, and large storage reservoirs (glacier ice and seasonal snowpack). Because of these large amplitudes and volumes, modest changes in meteorological forcings and landscape characteristics have the potential to produce significant changes in the timing and volume of runoff produced by these basins. This runoff is an important boundary condition for nearshore marine ecosystems and thus, constraining future changes in coastal runoff is a necessary first step for examining future changes to nearshore oceanography and ecology in GOA waters.

The southern Alaska coastline spanning the GOA receives large amounts of precipitation (an area-averaged annual value of 1.75–2.15 m, depending on the climate product) [Beamer et al., 2016] and is characterized by ice covered mountains, rainforest ecosystems, and marine estuaries and fjords. GOA glaciers account for ~10% of Earth's glacier area outside of the ice sheets and their peripheral glaciers [Pfeffer et al., 2014], and collectively are losing mass at a rate of  $-75 \pm 11 \text{ Gt yr}^{-1}$  [Larsen et al., 2015]. Beamer et al. [2016] calculated

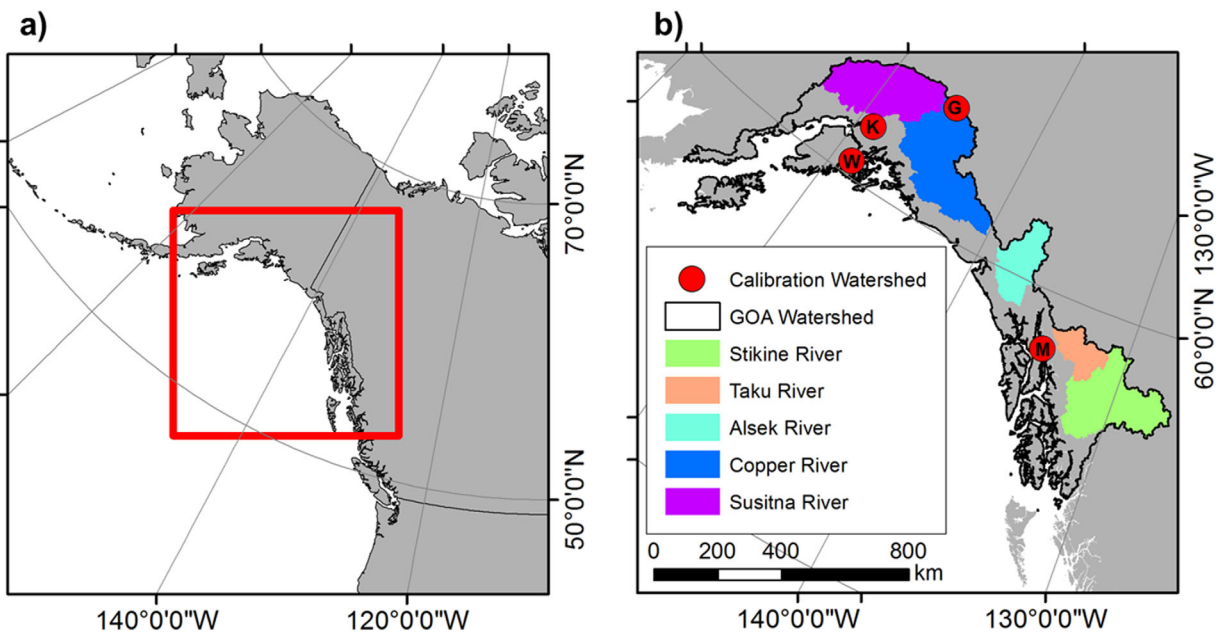


**Figure 1.** (a) Site map of northeastern Pacific Ocean with thick red line indicating extent of other panels and (b) Gulf of Alaska (GOA) domain with major inland drainage basins and red dots indicating following calibration watersheds with paired streamflow/glacier mass balance measurements: Knik River/Eklutna Glacier (K), Wolverine Creek/Wolverine Glacier (W), Pheian Creek/Gulkana Glacier (G), and Mendenhall Glacier/Mendenhall River (M).

an average freshwater flux of  $760 \pm 60 \text{ km}^3 \text{ yr}^{-1}$  (annual runoff depth of  $1.8 \pm 0.14 \text{ m}$ ) from the GOA watershed over the period 1980–2014, composed, on an annual basis, of 63% snowpack runoff (snowmelt and rain-on-snow), 20% rainfall, and 17% bare ice melt. Glacier volume loss (GVL) contributed 8% of the total average freshwater flux.

Climate models predict that the GOA will become warmer and wetter in the future [McAfee et al., 2014], leading to significant reductions in snowpack and glacier extent [Bliss et al., 2014; Huss and Hock, 2015; McGrath et al., 2017]. Increased precipitation and air temperature, decreased snow/rain fraction [McAfee et al., 2014], changes in land cover [Bieniek et al., 2015a; McGrath et al., 2017], and glacier-derived runoff [O’Neel et al., 2015] have the potential to drive large downstream changes in the timing, magnitude, and composition of the freshwater discharge to the GOA.

There have been several previous studies of the linkages between climate, glacier, and hydrologic change in Alaska. Many of these have focused on individual glaciers or have been regional studies of glacier-only surfaces. Bliss et al. [2014] used a temperature-index model and an ensemble of 14 general circulation models (GCMs) to simulate projected changes in glacier cover and runoff for regional subsets of Alaska. For the representative concentration pathway (RCP) 4.5 scenario, reductions in both glacier volume and area resulted in a decrease in annual glacier runoff of 30% between the periods 2003–2022 and 2080–2099. Huss and Hock [2015] also used a temperature-index model to model the surface mass balance for each 10 m elevation band for all glaciers globally, including Alaska. Their model was driven with monthly temperature and precipitation projections from 14 GCMs across three emissions scenarios (RCP 2.6, 4.5, and 8.5). They found that between 2010 and 2100 the total glacier volume for the Alaska region, currently  $\sim 16,400 \text{ km}^3$  water equivalent, decreased by 42% and 58% for RCP 4.5 and 8.5 scenarios, respectively. These studies provide a valuable yet incomplete understanding of the hydrology in complex coastal mountain watersheds such as the GOA. For example, Bliss et al. [2014; their Figure 8] showed little change in runoff timing from present day to 2100, which was due to their consideration of water yields from glacier surfaces only. They did not consider runoff that results from snowmelt and rain in the deglaciated area as the glacier retreats, which they anticipate would compensate for the reduction in glacier runoff at fixed points (e.g., stream gauge) downstream of the glacier. Huss and Hock [2015] focused exclusively on glacier change, which constrains the annual runoff contributions from long-term changes in glacier storage, but does not provide information on timing of runoff (seasonal hydrograph) or on other contributions (rainfall and snowmelt) to runoff.

The current study considers a more complete set of hydrologic processes and provides insight into the drivers of hydrologic change in the GOA. It extends a process-based historical (1980–2014) study [Beamer *et al.*, 2016] that modeled runoff from both glacier and land surfaces and partitioned fluxes into (rainfall versus snowfall) and out of (direct runoff, rain-on-snow, snowmelt, ice melt, sublimation, and evapotranspiration) the GOA watershed. Here we quantify the changes in coastal runoff that will occur due to increases in precipitation and temperature, and decreases in glacier cover. We do this by varying these forcings both individually and in tandem. We are particularly interested in (i) how climate model variability propagates through the hydrologic system, (ii) the physical mechanisms leading to changes in partitioning (e.g., do increases in snowpack runoff come from increases in snowpack itself, or in rain-on-snow events), and (iii) the relative contributions of meteorological and landscape changes to runoff changes.

## 2. Study Area

The GOA drainage basin was delineated with the coastal boundary running from the Alaska-Canadian border to Wide Bay on the Alaskan Peninsula (Figure 1). This drainage has a total area of 420,300 km<sup>2</sup> (~72,000 km<sup>2</sup> glacier cover) [Pfeffer *et al.*, 2014], with an annual average precipitation of 2.0 m arriving primarily in the autumn and winter as snow, with amounts in excess of 8.0 m in the southeastern panhandle [Beamer *et al.*, 2016].

The historical (1980–2014) study of Beamer *et al.* [2016] showed that the small coastal watersheds (areas < 1000 km<sup>2</sup>) made up 34% of the total area and contributed 48% of the annual runoff volume and 40% of the glacier runoff volume. In that paper and the present one, “glacier runoff” is defined as all runoff coming from glacier surfaces (rain, snowmelt, and ice melt). Midsized watersheds (between 1000 and 10,000 km<sup>2</sup>) made up 15% of the total area and contributed 19% of the total runoff and 29% of the glacier runoff volume. The large inland watersheds (>10,000 km<sup>2</sup>, Figure 1b) made up the remaining 51% of the area, 33% of total runoff, and 31% of the glacier runoff volume. The runoff into the Gulf of Alaska is therefore dominated by small (typically ungauged) watersheds near the coast characterized by high glacier cover and high precipitation rates.

## 3. Data and Methods

### 3.1. Hydrologic Model

There are many options for regional modeling of hydrologic processes, including conceptual and energy-balance approaches [Mosier *et al.*, 2016]. Conceptual models (e.g., temperature-index) lump multiple energy fluxes into a single term that is typically parameterized in terms of temperature. This is advantageous in terms of reducing both computational effort and the complexity of the required input data fields. Energy-balance methods represent individual fluxes and generally have greater input data requirements (wind speed, relative humidity, radiative fluxes, etc.). The increasing availability and spatial resolution of gridded weather reanalysis products is diminishing the potential “drawback” of these data intensive models. The potential advantage of energy-balance methods is that the relative contributions of individual energy fluxes can vary in time and space [Kustas *et al.*, 1994] and this variability can be lost in models that lump fluxes and parameterize them by a single variable (temperature).

Here we adopt the energy-balance model approach of Beamer *et al.* [2016] which uses an integrated suite of gridded meteorological (MicroMet) [Liston and Elder, 2006a], energy-balance snow and ice melt (SnowModel) [Liston and Elder, 2006b], soil moisture and evapotranspiration (SoilBal) [Beamer *et al.*, 2016], and linear-reservoir runoff routing (HydroFlow) [Liston and Mernild, 2012] models to simulate the pathways of water from precipitation input to coastal runoff. Model calculations were done at 1 km spatial resolution and 6 h temporal resolution for the future (2070–2099) period. In addition to analyzing the modeled water balance and snowpack, we partition the modeled runoff into elements of direct rainfall on snow-free surfaces, glacier ice melt, snowmelt, and rain-on-snow (ROS) runoff. ROS runoff was calculated as the runoff occurring from rainfall on a saturated snowpack. Runoff from direct rainfall and ROS are driven by precipitation phase (rain) and snowpack cover and conditions (density), distinct from snow and ice melt, which are driven by the energy-balance calculations in SnowModel. We note that in Beamer *et al.* [2016], the snowmelt and ROS runoff is lumped into a single snowpack runoff term. Output was subsequently spatially aggregated to the GOA watershed and temporally aggregated to produce a 30 year climatology. The model

components are only briefly reviewed here; readers are directed to *Beamer et al.* [2016] and the original publications for full details.

MicroMet [*Liston and Elder*, 2006a] distributes meteorological parameters (temperature, precipitation, relative humidity, and wind speed and direction) from weather stations or reanalysis grid centers to the spatial resolution of the DEM and land cover grids. Incoming solar and longwave radiation input data are calculated with additional MicroMet submodels, considering the influence of temperature, humidity (cloud cover), and topographic slope and aspect.

SnowModel [*Liston and Elder*, 2006b] uses the meteorological output from MicroMet to compute the full evolution of snow water equivalent (SWE) using an energy-balance approach. The processes in SnowModel include: (1) accumulation from snow precipitation; (2) blowing-snow redistribution and sublimation; (3) snow-density and mass transfer evolution; and (4) snowpack ripening, refreezing, and melt water flow. In this study, the surface energy balance and associated hydrologic fluxes were modeled on a 6 h time step to capture the diurnal fluctuations in snowmelt and ice melt, including hydrologically important rain-on-snow events. The model does not include dynamic adjustments to the glacier cover. As a result, this model suite is able to model the response (runoff) of a fixed glacier cover to climatic inputs, but is unable to evolve the glacier cover directly.

The SoilBal submodel for SnowModel was developed by *Beamer et al.* [2016]. First, potential evapotranspiration (PET) calculations based on air temperature, top-of-canopy net radiation and the Priestley-Taylor equation [*Priestley and Taylor*, 1972] were included. Second, routines were added to solve a soil water balance [*Flint et al.*, 2013]. SoilBal produces daily grids of actual evapotranspiration (ET), surface runoff, and base flow runoff. The resulting surface runoff and base flow output are then used as input to the runoff routing model.

Finally, HydroFlow [*Liston and Mernild*, 2012] simulates transport of runoff produced from rainfall, snowmelt, ice melt, and base flow across glaciers and land to downslope areas and basin outlets. A coupled system of equations solves for fast-response and slow-response flow and the final solution yields a discharge hydrograph for each model grid cell. Summation of the hydrographs of all coastal grid cells provides the discharge of the entire GOA basin. Results for other watersheds (e.g., a particular bay/fjord and the watershed draining to a given stream gauge) are obtained by aggregating the runoff from the grid cells of interest.

### 3.2. Model Input Data

The 1 km USGS Hydro1K North America data set was selected as the digital elevation model (DEM). Baseline vegetation classes for each grid cell were obtained from the 250 m North American Land Change Monitoring System (NALCMS) Land Cover 2005 map, regridded to align with the elevation grid. Additionally, it was necessary to adjust the vegetation classes to be consistent with the classification scheme defined in *Liston and Elder* [2006b]. Soil texture data were obtained from the gridded Harmonized World Soil Dataset (HWSD; Version 1.2) [*Fischer et al.*, 2008]. Finally, glacier extent was obtained from the Randolph Glacier Inventory (RGI; Version 3.2) [*Pfeffer et al.*, 2014]. The RGI coverage has a total glacier area of 72,392 km<sup>2</sup> in the delineated GOA drainage. While the NALCMS has a “snow and ice” classification, the RGI data are more current and more accurately represent ice cover. Grid cells that were “snow and ice” according the NALCMS but not the RGI were assigned bedrock classifications instead.

#### 3.2.1. Climate Forecast System Reanalysis

For baseline hindcast simulations we used the Climate Forecast System Reanalysis (CFSR; Versions 1 and 2) of the National Centers for Environmental Prediction (NCEP). Taken together, these data span the period 1979 to present (1 January 2011 separates the two versions). The reanalysis grid we used has spatial and temporal resolutions of 0.5° and 6 h, respectively [*Saha et al.*, 2010], with ~1100 grid points in the GOA model domain. *Beamer et al.* [2016] considered a total of four reanalysis products and determined that CFSR provided the most accurate regional simulations compared to GRACE satellite data in terms of annual amplitudes of regional water storage and long-term losses (ice loss) in the GOA region. The identification of CFSR as the leading reanalysis product is consistent with the comparative study of reanalysis products by *Lader et al.* [2016].

#### 3.2.2. Model Calibration

The distributed hydrologic model used in this study has a large number of parameters. To inform the selection of model parameters, a phased approach was adopted as described in *Beamer et al.* [2016] and only

summarized here. Simulations were carried out for four catchments (that contain Wolverine, Gulkana, Men- denhall, and Eklutna glaciers; see symbols in Figure 1) that sample the major hydrologic regimes found in the region (rainfall, snowmelt, and glacially dominated), and where glacier mass balance measurements and streamflow measurements were simultaneously available. Beamer *et al.* [2016] demonstrated that model results were most sensitive to four model parameters: precipitation lapse rate ( $\gamma$ ), glacier ice albedo ( $\alpha_{ice}$ ), and fast and slow-response times ( $k_f$  and  $k_s$ ). The lattermost parameters represent (i) the time scale of channel flow in streams and through glaciers and (ii) the time scale of transport through snow and ice matrices, and soil.

Validation simulations using the best set of model parameters produced statistically significant ( $p < 0.001$ ) coefficients of determination ( $r^2$ ) values of 0.63–0.77 for seasonal (winter and summer) point glacier mass balance at the four monitored glaciers and Nash Sutcliffe efficiency (not seasonally adjusted) values of 0.85–0.91 for monthly streamflow time series at the four stream gage stations. A partial listing of model parameters and their chosen values for this study is given in Appendix A.

### 3.2.3. Future Climate Data

There are numerous strategies for future climate data in studies of hydrologic change. The simplest approach [e.g., Engelhardt *et al.*, 2015] is to impose spatially and seasonally constant changes in precipitation and temperature. More recent efforts have sought to preserve the spatial and temporal (seasonal; inter-annual) variability present in projections of future climate. GCM spatial resolution is typically coarse; the average resolution for the models in the Coupled Model Intercomparison Project Phase 5 (CMIP5) is just under  $2^\circ$ . Some studies [e.g., Bliss *et al.*, 2014; Huss and Hock, 2015] have used this native resolution while others have downscaled [see Fowler *et al.*, 2007 for a review] the GCM data to a finer resolution using statistical [e.g., Immerzeel *et al.*, 2012] or dynamical methods [e.g., Shrestha *et al.*, 2013]. Similar choices must be made with temporal resolution. GCM output is commonly available at a subdaily time step, although users often coarsen it to daily or monthly increments [Bliss *et al.*, 2014; Huss and Hock, 2015].

At the time of this study, high spatial resolution dynamically downscaled CMIP5 GCM data were not available for the Alaska region. Bieniek *et al.* [2015b] describe their dynamic downscaling of the ERA-Interim product for Alaska and note their pending future extensions to GCM output. With that data not yet available, we adopted a hybrid approach to preparing our future climate data. This approach retains the  $0.5^\circ$  spatial resolution of the CFSR reanalysis product but perturbs both the precipitation and temperature fields based on historical and future GCM climatologies. This approach by definition retains the high-frequency temporal characteristics of the historical CFSR time series and is therefore not suited for assessing changes to peak flow characteristics or other quantities dependent on the temporal structure of the signal. However, it does allow us to analyze the changes to the mean monthly runoff patterns to long-term shifts in climate. We note that our approach is a variant of the so-called “constant scaling” described by Mpelasoka and Chiew [2009]. Those authors compared numerous empirical scaling methods and found that the variability among methods (~5%) was far less than the variability among GCMs (~40%).

Our specific approach uses GCM products prepared by the Scenarios Network for Alaska + Arctic Planning project (SNAP; <https://www.snap.uaf.edu/>). SNAP provides downscaled temperature and precipitation monthly time series (as well as 30 year monthly climatologies) using CMIP5 GCM data. The GCM data are statistically downscaled to high spatial resolution (2 km) but low temporal resolution (monthly) grids. The five GCMs provided by SNAP were the top performing models (lowest bias) according to Walsh *et al.* [2008]. SNAP also provides the 5-model mean as a sixth product.

For each combination of GCM product (six total) and RCP scenario (two) the gridded climatologies of mean monthly air temperature and total precipitation from historical (1980–2009) and future (2070–2099) periods were acquired from SNAP. The future and historic temperature climatologies were differenced to generate the climate anomaly grids; one per month or 12 in total. In the case of precipitation, the ratio between the future and historic climatologies was computed in order to obtain the anomaly grids. These 2 km anomaly grids were then resampled to match the  $0.5^\circ$  spatial resolution of CFSR, and then applied to the 6 h data set, by month, in order to create future data sets with the correct spatial and seasonal distribution of mean variables. Based on this approach, the temperature data shift only in the monthly mean, while the precipitation data shift both in the monthly mean and standard deviation. We note that this approach does not directly alter the radiation, relative humidity, and wind inputs. However, MicroMet calculates the radiation inputs based on other available variables.

### 3.2.4. Future Glacier Cover Extent

The glaciers in the GOA are anticipated to retreat significantly by the end of the century [e.g., Huss and Hock, 2015; McGrath *et al.*, 2017]. Given that the timing and magnitude of runoff from glacier catchments depend strongly on the areal extent of glacier ice, it is necessary to model future glacier extent prior to conducting studies to forecast hydrologic responses. Despite the availability of physically based transient glacier evolution approaches [e.g., Clarke *et al.*, 2015, Ziemen *et al.*, 2016], the glacier melt modules in many hydrologic models use a static glacier cover that is updated assuming glaciers to be in equilibrium with representative climate conditions according to the Paul *et al.* [2007] accumulation area ratio (AAR) method [Schaeffer *et al.*, 2005; Bavay *et al.*, 2013]. The AAR is the ratio of the area of the accumulation zone of a glacier to the total area of a glacier. In this study, since our goal is to explore the sensitivity of the hydrologic cycle to plausible, future landscapes produced by specific climate forcings, rather than to transiently evolve glacier cover over the study interval, the method of Paul *et al.* [2007] was adopted.

We derived 10 m hypsometric bins for each individual glacier in the Alaska region using the RGI [Pfeffer *et al.*, 2014] and a multisource DEM (90 m grid) consistent with the inventory [Kienholz *et al.*, 2015]. This DEM was at a higher resolution than the hydrological model grid (GTOPO; 1 km), which allowed for accurate delineation of individual glaciers. The method of Paul *et al.* [2007] was then used to change glacier extent as a function of changes in equilibrium line altitude (ELA) and a steady state AAR ( $AAR_0$ ). The ELA is the altitude at which ablation is balanced by accumulation. We used an  $AAR_0$  of 0.65, based on the mean observed value from four Alaska benchmark glaciers in Mernild *et al.* [2013] to determine the initial ELA of each glacier. We then subsequently raised the ELA by 200 and 400 m, respectively, for RCP 4.5 and 8.5. These increases were taken from the differences between the mean 2010 ELA and the mean 2070–2100 ELA for the Alaska region glaciers (~90% of which are in the GOA) reported by Huss and Hock [2015; their supporting information Figure S9]. Following Paul *et al.* [2007], future glacier cover masks were created by sequentially removing the lowest elevation bins until the glacier returned to the  $AAR_0$  value of 0.65 (with the accumulation area minimum elevation defined by the new ELA). A second set of masks was produced by using the above ELA increases, but instead implementing the transient AAR values for 2070–2100 reported by Huss and Hock [2015; their supporting information Figure S10]; 0.44 for RCP 4.5 and 0.34 for RCP 8.5. This additional degree of freedom in our experimental matrix allowed us to specifically test the sensitivity of runoff and its partitioning to future land cover.

The four updated 90 m glacier cover grids were coarsened back to the 1 km hydrological model grid and used to generate revised SnowModel land cover files. Each glacier ice cell that was removed due to ELA increase was replaced with a bare ground cover cell; we did not account for vegetation/soil succession in this study. We also kept our DEM input constant, not considering surface lowering due to glacier thinning. The glacier cover masks were kept constant during the 30 year modeling period, such that we do not account for additional glacier retreat during the model period.

### 3.2.5. Model Run Configuration

We performed a series of tests with the different climate/land cover combinations to quantify the sensitivity of future GOA runoff to perturbations in climate and glacier cover. The first series of tests perturbed climate forcings, but kept the glacier cover fixed at present day. Five individual GCMs and two RCP scenarios were used, resulting in 10 model runs that provide information on runoff variability due to GCM variability. The second series of tests retained historic climate (CFSR) but altered the glacier cover as described above (two RCP scenarios and two future ELA values), resulting in four model runs. A third series of tests paired the perturbed climate (two RCP scenarios) with the updated glacier cover (two ELA scenarios per RCP). For these final model runs, only the 5-model mean climate forcing was used, instead of the individual GCMs, so this final set adds four model runs. This systematic approach, using a total of 18 model runs, allowed us to determine the main controls on changing runoff into the GOA at the end of the 21st century.

## 4. Results

### 4.1. Historical Conditions

Beamer *et al.* [2016] found that CFSR produces a current (1980–2014) mean annual runoff volume of  $760 \text{ km}^3 \text{ yr}^{-1}$  and this serves as the baseline simulation for this study. Approximately 38% of the annual runoff volume is derived from glacier runoff. The seasonal runoff is partitioned into four surface water sources:

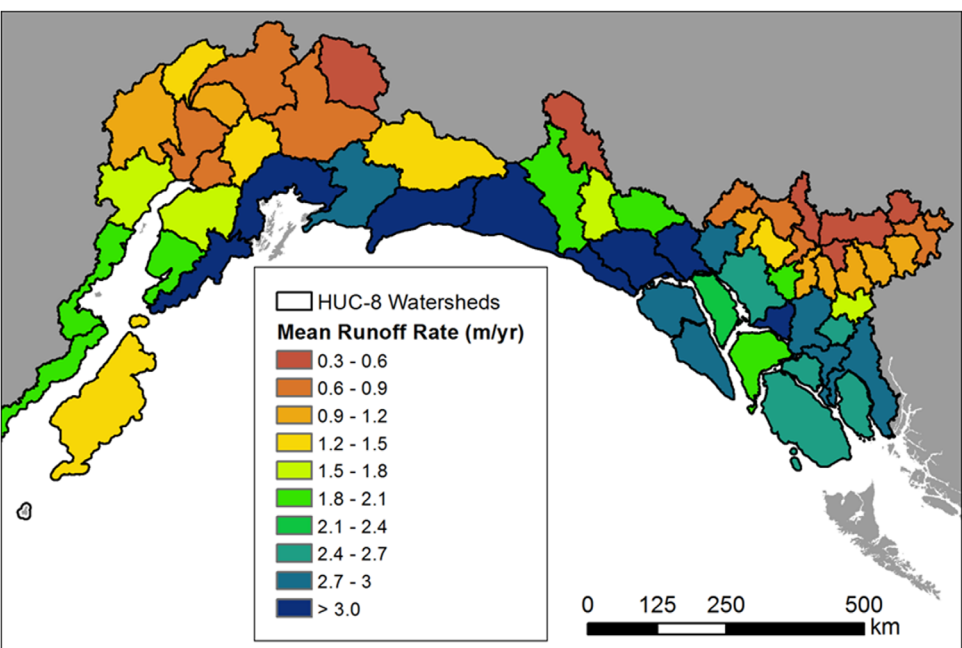


**Figure 2.** Map of mean annual runoff rate ( $\text{in m yr}^{-1}$ ) for CFSR-forced simulations aggregated to the HUC8 (USA regions) and unofficial NHN WorkUnits (1:50K) and official Canadian Fundamental Drainage Areas (FDA 1:1M) (Canadian regions) watersheds within the GOA region.

snowmelt, rain-on-snow (ROS) from a saturated snowpack, direct rainfall on snow-free land and ice surfaces, and glacier ice melt from snow-free glacier ice surfaces. Snowmelt dominates from April to July (51% of annual total), ROS contributes significantly throughout the winter and spring months (12% of total) while ice melt and rainfall dominate in August and September (17% and 20% of annual total, respectively). Runoff to the GOA exhibits a gradient of decreasing runoff depths with distance from the coast (Figure 2), which is similar to the pattern of precipitation inputs [Beamer et al., 2016]. Note that the watersheds in Figure 2 are a combination of USGS HUC8 boundaries (USA regions) and unofficial NHN WorkUnits (1:50K) and official Canadian Fundamental Drainage Areas (FDA 1:1M) (Canadian regions).

#### 4.2. Effects of Climate Forcing

##### 4.2.1. Changes in Precipitation and Temperature

Figures 3a and 3b show the climatology of GOA aggregated mean air temperature and precipitation for historical conditions (CFSR) along with the future (2070–2099) average of the 5-model ensemble of runs for RCPs 4.5 and 8.5. The vertical bars indicate the standard deviation of the results from the 5-model ensemble. Both temperature and precipitation show increases throughout the year and both variables experience larger increases for RCP 8.5 than RCP 4.5. Spatially averaged mean annual values of precipitation and temperature are provided in Table 1. Temperature increases are largest in November and precipitation increases are largest in October.

As a result of the increased air temperatures, the partitioning of the precipitation becomes more rain dominated, with the fraction of annual precipitation falling as snow decreasing substantially (Figure 3c and Table 1). Increased precipitation partially offsets the reduced snow-rain fraction, but the annual snowfall volume still decreases substantially from historical volumes. For the future simulations, peak SWE still occurs in April, but SWE volumes are greatly reduced (Figure 3d and Table 1).

##### 4.2.2. Changes in Runoff

Figure 4 summarizes the mean annual hydrograph for the baseline run, and the runs where climate forcings have been altered but the modern RGI glacier cover has been retained. Additionally, Table 2 summarizes all runoff results in this study, both in terms of volumes and in terms of percentage changes from the baseline run. The total annual runoff volume increases by 25% and 46% for RCP 4.5 and 8.5, respectively, with glacier surfaces providing approximately 75% of the observed increases. As with Figure 3, vertical bars indicate the variability among the five GCMs. The coefficients of variation of the runoff are more than twice those of the

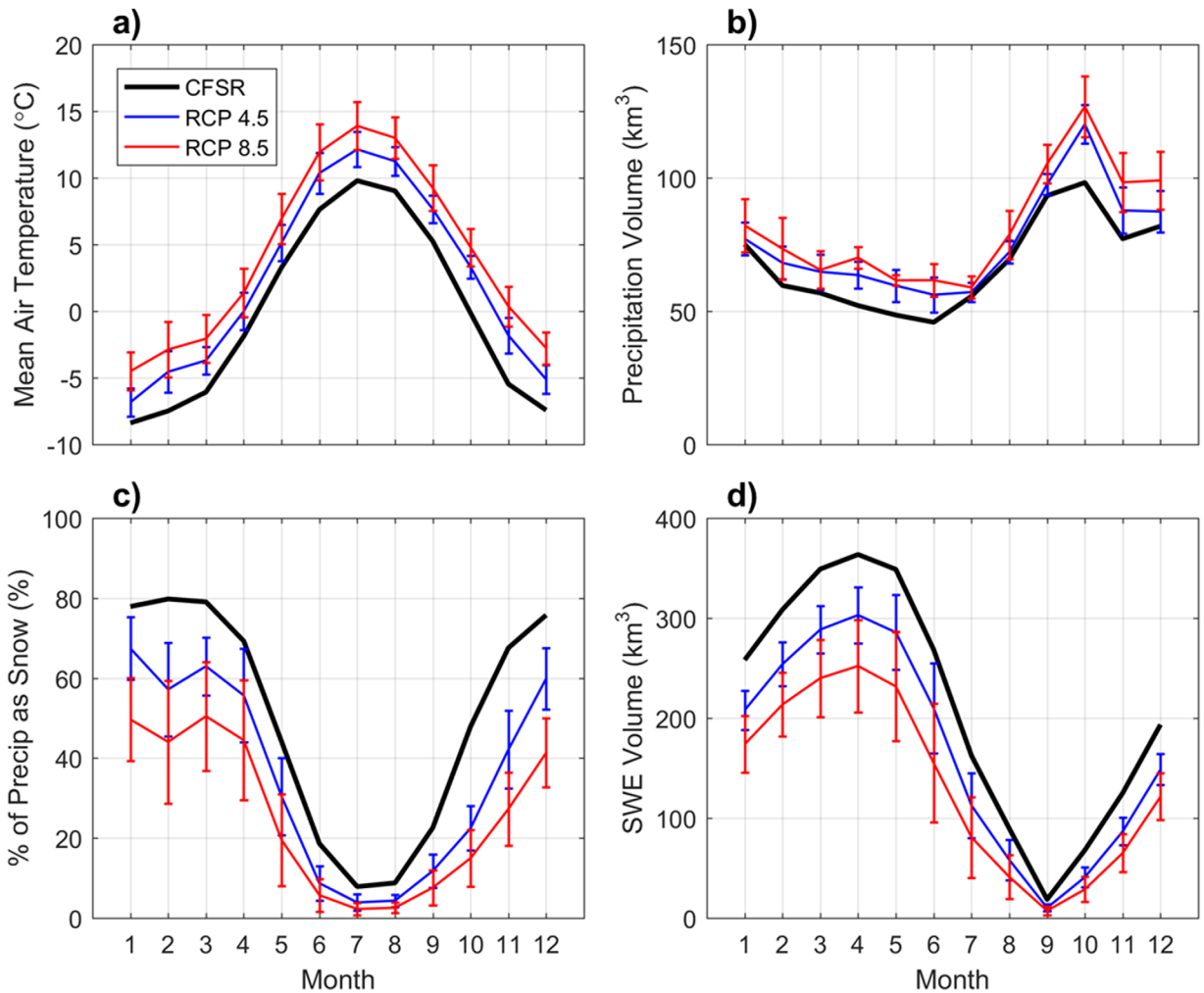


**Figure 3.** (a) Mean monthly air temperature, (b) precipitation, (c) snowfall fraction, and (d) snow water equivalent of the snowpack aggregated to the GOA basin for historical (black line), RCP 4.5 (blue line), and RCP 8.5 (red line) conditions. For future scenarios, the solid line gives the intermodel mean result and the error bars indicate one standard deviation.

precipitation inputs. In other words, the variability in precipitation input is “amplified” as the water is routed through the hydrologic cycle and across the landscape to the coast. Seasonally, winter flows increase substantially, with mean December–February (DJF) runoff increasing by 93% and 201% for RCP 4.5 and 8.5, respectively. There is a broadening of the summer runoff peak, particularly from June through October, due to a combination of enhanced glacier-derived runoff and rainfall runoff.

**Table 1.** Mean Annual Values of Weather Inputs and Snowpack Aggregated to the GOA Drainage for Historic (1980–2014) and Future (2070–2099) Scenarios Using the RGI Glacier Cover<sup>a</sup>

Climate Product	Air Temp. (°C)	Total Precip. (km <sup>3</sup> yr <sup>-1</sup> )	Snowfall (km <sup>3</sup> yr <sup>-1</sup> w.e.)	Rainfall (km <sup>3</sup> yr <sup>-1</sup> )	Peak SWE Volume (km <sup>3</sup> w.e.)
CFSR	-0.13	810	410	400	365
RCP 4.5	2.3 ± 1.0	910 ± 35	320 ± 40	590 ± 70	305 ± 25
	2.5	12%	-22%	48%	-17%
RCP 8.5	4.1 ± 1.5	980 ± 45	250 ± 55	730 ± 100	255 ± 40
	4.3	21%	-40%	83%	-30%

<sup>a</sup>For historic CFSR model output, only the mean annual value is shown; for future scenarios, both the 5-model mean and standard deviation are presented. The second row in the RCP 4.5 and 8.5 cells provide the relative (for temperature) and percentage (for other variables) change in mean from the baseline (historic CFSR) run. Snow values are given as water equivalent (w.e.).

### 4.3. Effects of Glacier Cover

#### 4.3.1. Changes in Glacier Cover

Figure 5 shows the spatial coverage of current and altered glacier cover for 200 and 400 m ELA increases using the AAR<sub>0</sub> (Figure 5a) and transient AAR (Figure 5b) assumptions. Note that the spatial extent has been zoomed in to focus on the region of greatest glacier coverage (i.e., Prince William

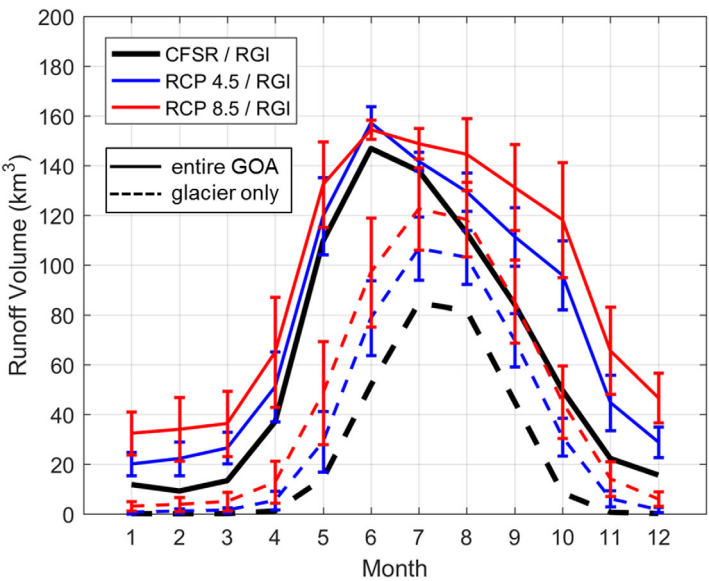


**Figure 4.** Climatological hydrograph for the GOA watershed for historical and future climate scenarios with present-day glacier cover. Solid lines are for the entire watershed, dashed lines are for glacier cells only. The simulations were forced separately with the five GCMs; the solid line gives the intermodel mean result and the error bars indicate one standard deviation, providing a measure of the variability in runoff due to the uncertainty in future climate forcings.

cells with the transient AARs, which retain most of the low-elevation glacier cover, while the curves for  $\text{AAR}_0$  show a larger proportion of glacier cells at high elevations (Figure 6b). This is important since the retention of low-elevation glacier ice greatly increases the production of meltwater, and thus the glacier contribution to overall runoff.

#### 4.3.2. Changes in Runoff

Increasing the ELA by 200 to 400 m and using  $\text{AAR}_0$  and historical CSFR climate forcing, we find modest reductions in total runoff and dramatic reductions in runoff from glacier surfaces (Figure 7a and Table 2). Note that the lack of vertical bars in this figure is due to forcing the model runs with only the 5-model mean, rather than the five individual GCMs. Seasonally, the hydrograph changes are from June through October exclusively. The timing of this reduction is coincident with peak glacier runoff contributions and sig-

nals the loss of low-elevation glacier extent (Figure 6). For the case of transient AAR, the decrease in runoff is much less dramatic (Figure 7b) since more glacier ice remains at low elevations and thus produces meltwater in the present climate.

#### 4.4. Combined Effects of Climate and Glacier Cover Change

The final series of model runs used the perturbed climate and altered glacier cover together. As in section 4.3, we used only the 5-model mean for future climate. Figure 7c shows the results of future

**Table 2.** Mean Annual GOA Total Runoff Volumes and Glacier-Only Runoff Volumes (in Parentheses) in  $\text{km}^3 \text{yr}^{-1}$  for the Different Glacier-Climate Sensitivity Tests<sup>a</sup>

	Climate Forcing		
	CFSR	RCP 4.5	RCP 8.5
<b>Glacier Cover</b>			
RGI	760 (290)	<b>950 ± 80 (440 ± 70)</b> 25% (52%)	<b>1110 ± 130 (560 ± 120)</b> 46% (93%)
ELA + 200 (AAR = 0.65)	680 (160) -10% (-45%)	830 (250) 9% (-14%)	
ELA + 400 (AAR = 0.65)	650 (85) -14% (-71%)		865 (190) 14% (-34%)
ELA + 200 (AAR = 0.44)	730 (240) -4% (-17%)	905 (360) 19% (24%)	
ELA + 400 (AAR = 0.34)	705 (180) -7% (-38%)		980 (355) 29% (22%)

<sup>a</sup>Blank cells are combinations that were not run. Bold values indicate results (5-model mean and standard deviation) for ensemble runs with the five individual GCMs; other results are from runs completed with a single (CFSR reanalysis or GCM 5-model mean) forcing data set. The second row in each cell provides the percentage change in mean from the baseline (historic CFSR) run.

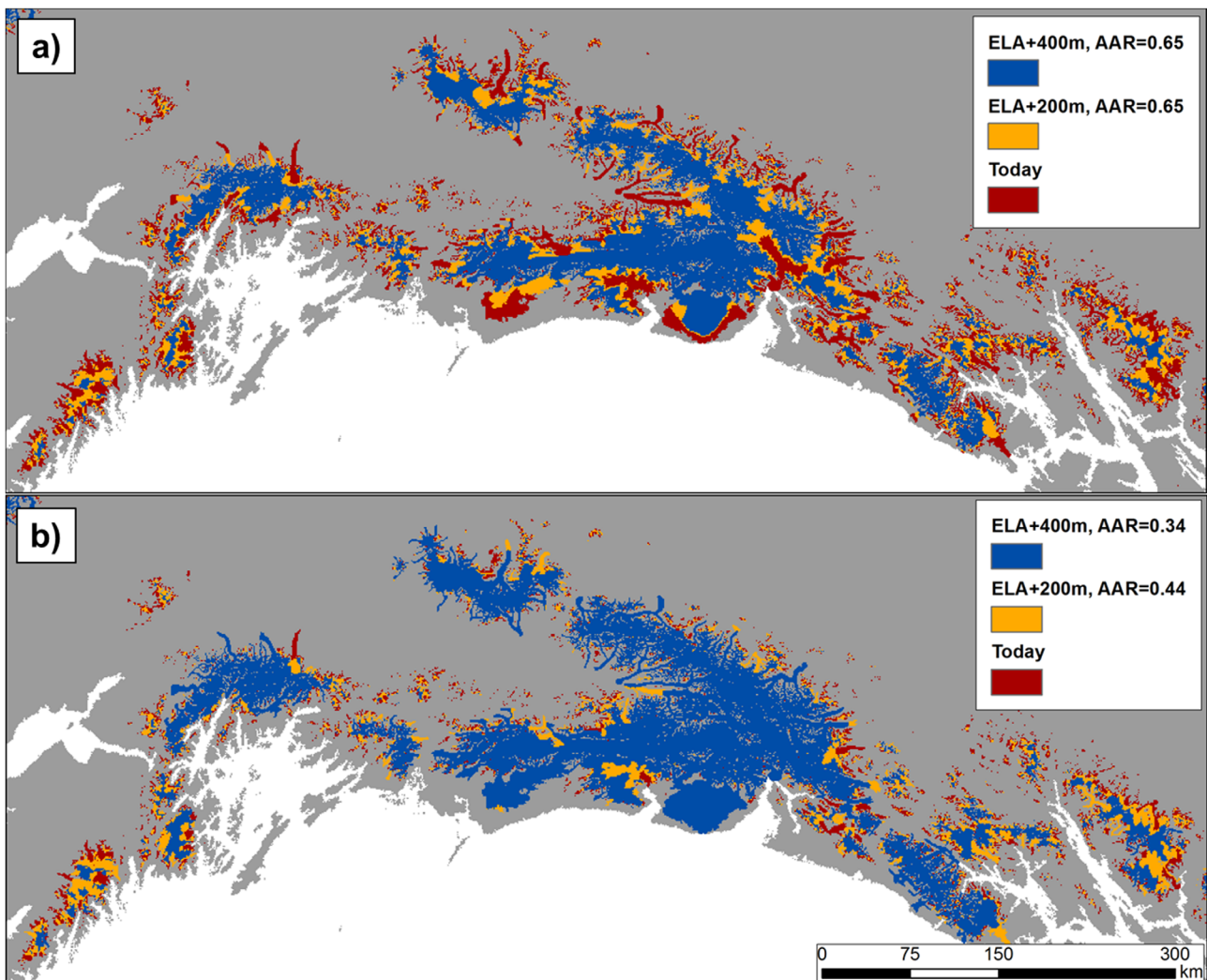


**Figure 5.** Distribution of glacier cells in the central portion of GOA for ELA increases of 200 and 400 m. (a) ELA increases assuming  $AAR_0$  of 0.65. (b) ELA increase assuming transient AAR values from Huss and Hock [2015].

climate paired with  $AAR_0$  glacier cover and Figure 7d shows the results for the transient AAR case. In both cases, there are substantial changes in the hydrograph compared to the baseline. Additionally, the hydrograph from the paired run differs considerably from the runs in which climate and glacier cover were varied individually (Figures 4, 7a, and 7b). The strong summer peak found in the baseline simulations is now weakened and the overall hydrograph begins to exhibit a bimodal distribution with a late spring peak due to snowmelt and an early autumn peak due to rainfall. The summer peak in the hydrograph (Figure 7c) is lost due to reduction in glacier ice at low elevation, and thus an overall reduction in glacier melt during this period. There are also strong increases in winter flows, with mean DJF runoff increasing by 92% and 197% for RCP 4.5 and 8.5, respectively. These increases, similar to what was seen in Figure 4, are due to a combination of effects including increased precipitation and warmer atmospheric temperatures that reduce the snow/rain fraction.

The effect of the assumed AAR is striking, both in terms of overall runoff volumes and the partitioning to different sources. The future hydrographs in Figure 7d are similar in shape to those in Figure 7c but show a weaker change in the summer. The glacier runoff is actually found to increase in the transient AAR case and this increase mitigates the reduction in glacier area that led to strong decreases in glacier runoff in the  $AAR_0$  case (Figure 7c). The total runoff volume increases in both AAR cases (Table 2), but the increases over the baseline predicted by the transient AAR case are roughly double those from the  $AAR_0$  case, because of

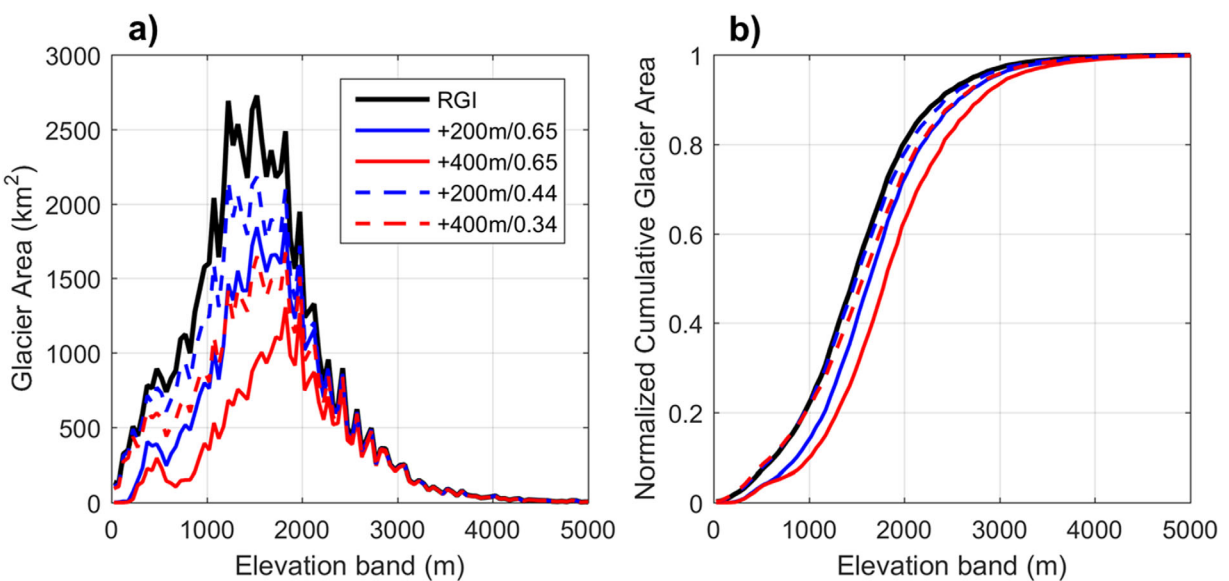


**Figure 6.** Glacier hypsometry based on 50 m elevation bands for various combinations of ELA increase and AAR. (a) Histogram of the glacier cell count in each elevation band from sea level to 6000 m asl and (b) cumulative distribution of glacier cells starting at sea level.

the substantial increase in runoff from both glacier and land surfaces. The increased runoff from glacier surfaces is due to higher ablation rates driven by warmer air temperatures and the increased runoff from land surfaces comes from increased liquid precipitation.

The model runs with an  $AAR_0$  of 0.65 (Figure 7c) produce late 21st century glacier runoff values similar to *Bliss et al. [2014]* and projected mass balance values similar to *Huss and Hock [2015]*. Model runs using the transient AAR values (Figure 7d) retain substantially more ice at low elevations, thereby producing large increases in glacier runoff and glacier volume loss rates that are inconsistent with these studies. This provides support for the  $AAR_0$  approach and we restrict our remaining results to this steady state case.

The partitioning of future runoff into the four hydrologic sources (glacier ice melt, snow melt, ROS, and direct rainfall) is presented in Figure 8. In the baseline case forced by the CFSR climate combined with RGI glacier cover (Figure 8a), the GOA runoff partitioning was dominated by snowmelt (51%), followed by combined rainfall runoff from direct rainfall and ROS (32%) and glacier ice melt (17%). For the RCP 4.5/ELA 200 scenario (Figure 8b), the annual GOA runoff partitions into 45% rainfall runoff, 41% snowmelt, and 14% glacier ice melt. For the RCP 8.5/ELA 400 scenario (Figure 8c), the annual GOA runoff partitions into 54% rainfall runoff, 35% snowmelt, and 11% glacier ice melt. For these future scenarios, rainfall runoff becomes a much larger contributor to the total runoff volume, snowmelt occurs earlier with a smaller overall contribution, and glacier ice melt decreases and becomes confined to higher elevation watersheds that retain glacier cover. The seasonal runoff hydrograph exhibits less month-to-month variability for future climate scenarios, with an increase in spring runoff from an earlier snowmelt, a smaller peak flow due lower midsummer meltwater runoff, and an increase in fall and winter runoff from more direct rainfall and ROS events.

#### 4.5. Hydrologic Regime Change

To briefly give context to the utility of this modeling work for local applications, we looked at the spatial variation of predicted changes in the hydrologic regime caused by changes in climate and glacier extent. Changes in timing, magnitude, distribution, and composition of streamflow can impact important species such as Pacific salmon and their riverine habitat. For example, more frequent winter floods can scour salmon eggs and increase sedimentation in spawning gravels [*Shanley and Albert, 2014*], and decreased summer flows can lead to warmer water temperatures and a decrease in spawning habitat [*Wobus et al., 2015*]. While our modeling is not designed to look at changes in peak flows, there are other key hydrologic parameters important for salmon habitat [*Wobus et al., 2015*] that our modeling can address. These include the timing (month) of maximum mean monthly runoff, magnitude of summer runoff, and magnitude of winter runoff. As an example, we focus on the first of these. A mean annual hydrograph was developed for

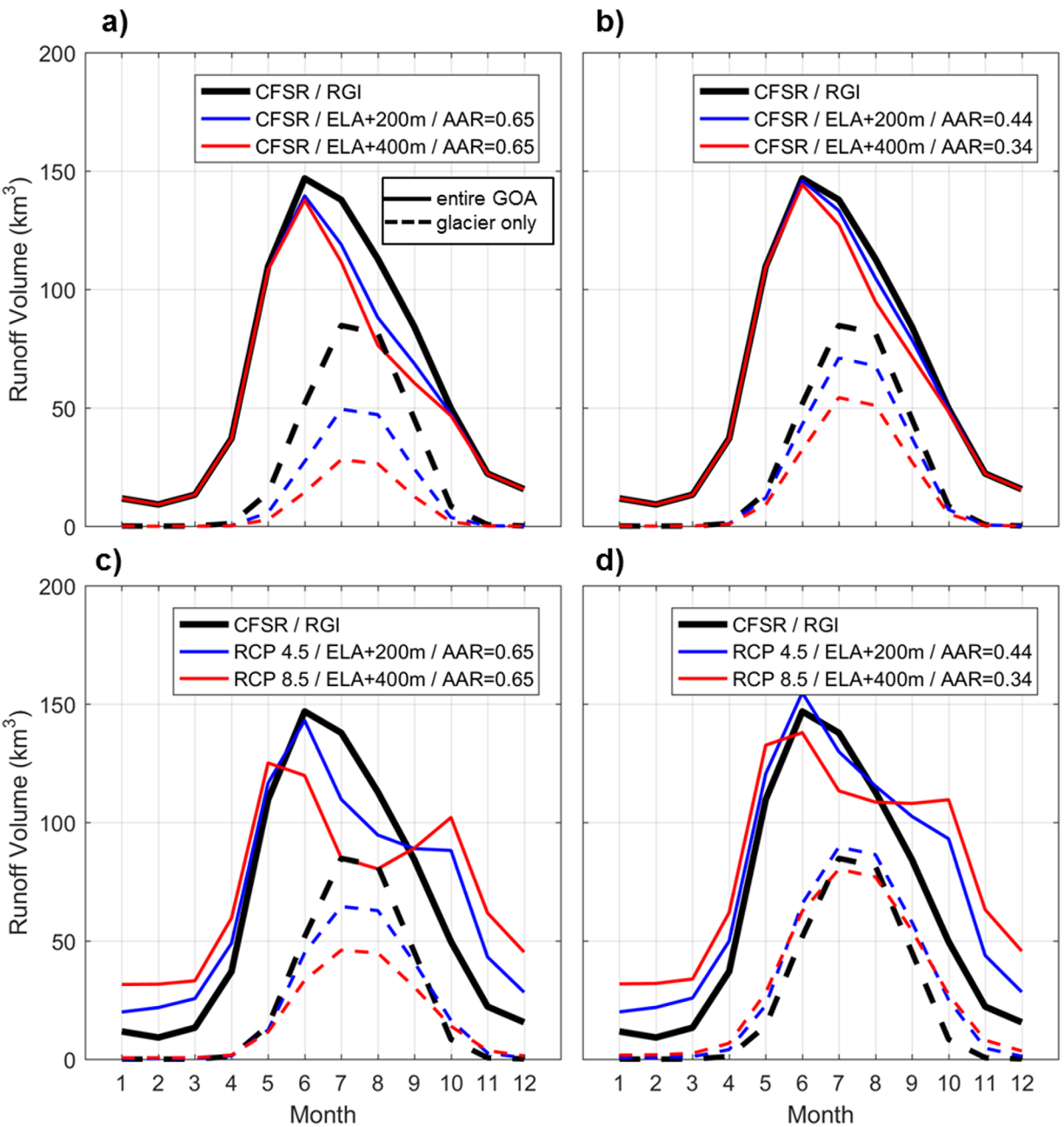


**Figure 7.** Climatological hydrograph for the GOA watershed using various climate-glacier cover scenarios. Solid lines are for the entire watershed, dashed lines are for glacier cells only. (a) Historic CFSR with  $AAR_0$  (0.65). (b) Historic climate with transient AAR values from Huss and Hock [2015]. (c) Adjusted climate and  $AAR_0$  (0.65). (d) Adjusted climate and transient AAR values from Huss and Hock [2015].

each watershed shown in Figure 2 for the baseline case and for the  $AAR_0$  RCP 4.5/ELA 200 and RCP 8.5/ELA 400 cases.

The month of peak runoff for the three model forcings are shown in Figure 9 (left). Annual runoff hydrographs, each month normalized as fraction of the annual total, from three watersheds (labeled (a), (b), and (c)) are presented in the right to highlight how the hydrographs change in different sectors of the GOA. These watersheds represent three distinct hydrologic regimes: (a) a snowmelt-dominated inland watershed with high mean elevation (1190 m) and low (4%) glacier cover (Figure 9a); (b) a hybrid (hydrograph contains both spring snowmelt and fall rainfall peaks) coastal watershed with low mean elevation (280 m) and no

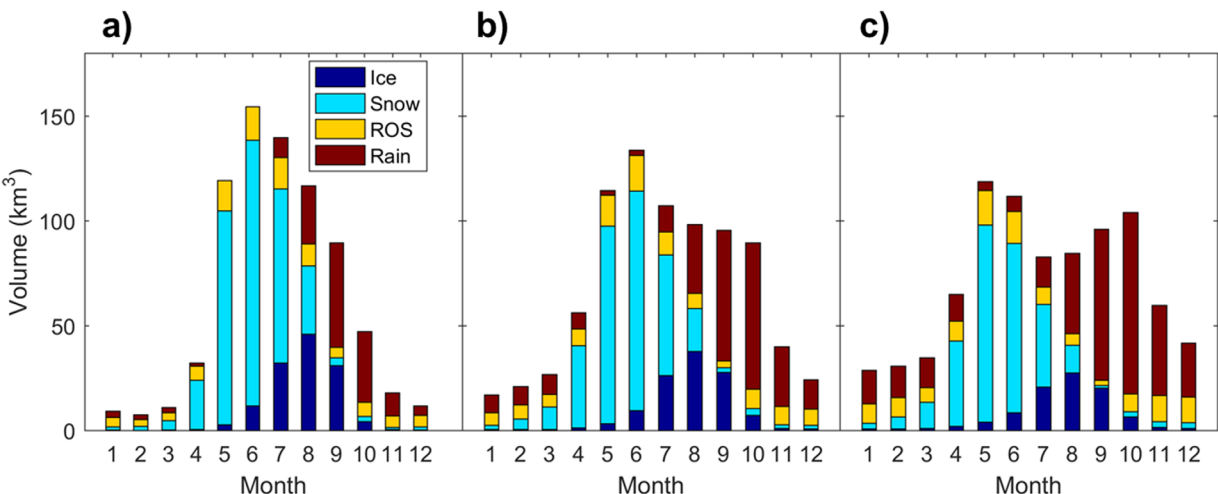


**Figure 8.** Stacked plots of mean monthly runoff volume from the GOA basin partitioned into following components: glacier ice melt, snow melt, rain-on-snow (ROS), and direct rainfall runoff. (a) Simulations driven with 1980–2009 CFSR and RGI glacier cover. (b) Climate forcing from 5-model mean RCP4.5 and glacier cover from 200 m ELA increase ( $AAR_0 = 0.65$ ). (c) Climate forcing from 5-model mean RCP8.5 and glacier cover from 400 m ELA increase ( $AAR_0 = 0.65$ ).

glacier cover (at the 1 km resolution of the model grid; Figure 9b); and (c) a glacially dominated coastal watershed with mean elevation of 550 m and high (31%) glacier cover (Figure 9c).

The snowmelt-dominated inland watershed (Figure 9a) historically had a spring runoff onset in May that peaked in June. Warmer air temperatures cause an earlier spring snowmelt onset that begins in April and peaks in May, and lower flows from June to August. The flows in October increase due to more rainfall runoff from increased precipitation input and higher rainfall fraction. The hybrid coastal watershed (Figure 9b) historically had both a spring snowmelt peak in May and a fall rainfall peak in October. Warming temperatures drive an increase in winter rainfall, which runs off immediately, and thus limits winter snow accumulation and drives an increase in runoff from October to March. Without available snowpack to melt and supplement summer flows, flows decrease dramatically from April to July and the future hydrograph is rain dominated. The heavily glaciated coastal watershed shows a dramatic flattening of the hydrograph (Figure 9c) due to a combination of warming temperatures and decreased glacier extent. Increased runoff from October to April is due to more precipitation falling as rain which runs off immediately rather than being stored as snowpack. The decreased flows from May to September are mainly due to loss of glacier melt contribution from the large reductions in glacier cover for this watershed (50% for ELA 200; 88% for ELA 400).

## 5. Discussion

### 5.1. Comparison to Previous Work

The century-scale projections in hydrologic model inputs (climate and glacier cover) and outputs (snow and streamflow) presented here are consistent with observations at the decadal to half-century time scale. *Bieniek et al.* [2014] analyzed weather data from 1949 to 2012 and found a clear increase in the statewide mean annual air temperature. They also found an increase in precipitation in the southern coastal regions during autumn and winter months. *Arendt et al.* [2009] also demonstrated widespread glacier mass loss and were able to correlate these losses with increases in summer temperatures.

*Hodgkins* [2009] studied streamflow changes in Alaska between 1947–1976 and 1977–2006; periods that correspond to the cool and warm phases of the Pacific Decadal Oscillation (PDO) [Mantua et al., 1997]. The warm phase is characterized by warmer and wetter conditions in Alaska and is therefore a proxy for the century-scale secular trends in temperature and precipitation predicted by GCMs. In glacierized basins, streamflow increases were observed in all months. At first, this may seem to contradict the result in Figure 9c, which was a glacierized basin. However, recall that the strong reduction in summer flows shown in Figure 9c is primarily due to the near total loss of glacier cover in that watershed. Because glacier geometries changed less dramatically during the periods examined by *Hodgkins* [2009], the streamflow changes for glacierized basins are more comparable to Figure 4 which showed the change in runoff due to changing

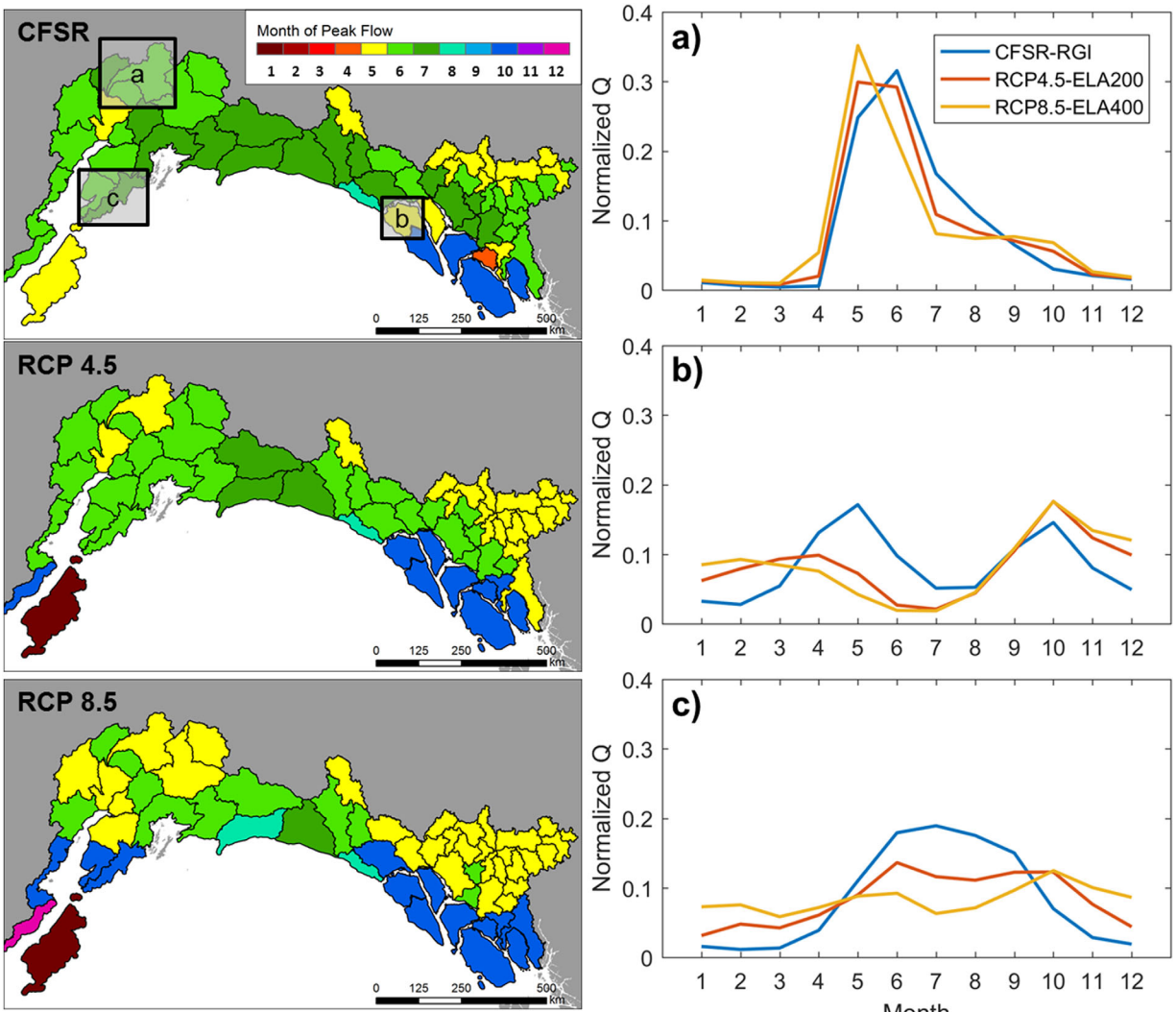


**Figure 9.** Maps of the month of peak flow from climatological hydrographs aggregated to GOA HUC8 watersheds. Normalized hydrographs for three climate-glacier cases from three HUC8 watersheds. Locations of three watersheds (a–c) shown in the (top left) CFSR.

climate, but fixed glacier cover. These results emphasize that the response of annual hydrographs to climate change for glaciated basins is strongly dependent on the time scale over which the change occurs. In non-glacierized basins, streamflow decreases were found in summer months, with increases in other months. The decreases in summer months can be attributed to earlier snowmelt and lack of glacier ice to sustain summer flows. These findings are consistent with the hydrographs shown in Figures 9a and 9b.

The findings in this study are also generally consistent with previous projection modeling studies. While no comparable regional study of the GOA exists, there have been relevant studies, using a wide variety of methodologies, throughout British Columbia and Alaska. *Shanley and Albert* [2014] developed regression equations for mean monthly flows in southeast Alaska. When applied to future climatologies, they found increased winter flows and a shift to earlier spring flows. *Schnorbus et al.* [2014] applied the Variable Infiltration Capacity (VIC) model [Liang et al., 1994] to three basins (two inland, one coastal) in British Columbia. Their results indicated that hydrograph timing would shift primarily due to changes in the dynamics of snow accumulation and melt. In the inland basins, hydrographs shifted to an earlier spring peak and in the coastal basin, the hydrograph shifted to a rain-dominated autumn/winter peak.

### 5.2. Reducing Uncertainty and Relevance to Other Glaciated Areas

The broad agreement in general trends between observations and modeling studies (and among modeling studies based on very different methods) is encouraging but also raises the question of how to best

constrain hydrologic projections in coastal mountain regions (e.g., improved model forcing versus improved model physics) [Huss *et al.*, 2010]. As summarized in Table 2, changes in meteorological inputs and glacier areal extent have opposite effects on runoff. When only the precipitation and temperature fields are changed (increased), runoff (both total and that from glacier surfaces) increases. When only the glacier cover is changed (reduced) runoff decreases. The changes to the model inputs have considerable uncertainty and this uncertainty propagates into uncertainty in the outputs including SWE and runoff [Sulis *et al.*, 2012]. Recall that Figures 3 and 4 provided vertical bars that described one standard deviation among the five GCMs considered in this study. Since total runoff changes are the difference between these two competing drivers, the potential outcome is a relatively small change subject to large uncertainty [e.g., Huss *et al.*, 2014].

One path toward reducing runoff uncertainty is in reducing weather forcing uncertainty, although there is some evidence that improvements in model physics and resolution from CMIP3 to CMIP5 did not produce noticeable convergence in the results among the ensemble of climate models [e.g., Knutti and Sedláček, 2013]. Greater dividends will likely be paid by efforts to accurately model future glacier extent. Recall from Table 2 that the two sets of experiments carried out with different AAR values for the 2070–2099 period produced opposite results in terms of changes in glacier runoff. In the case of the  $AAR_0$ , total runoff increased, but runoff from glacier surfaces decreased for both the RCP 4.5 and 8.5 simulations. In the case of the transient AAR, which left significant amounts of glacier ice at low elevations (Figure 5), both total runoff and runoff from glacier surfaces increased substantially from the baseline. Modeling a realistic glacier cover is of first-order importance and future work should model the glacier retreat in a more sophisticated manner.

Options for evolving the glacier cover, beyond the AAR method used in this paper, range from approaches that update the glacier extent using volume/area scaling [e.g., Radić and Hock, 2006; Radić *et al.*, 2013] to more complex models that apply normalized elevation change functions across the glacier geometry [Huss *et al.*, 2010; Huss and Hock, 2015] or explicitly model ice flow dynamics [e.g., Clarke *et al.*, 2015, Ziemen *et al.*, 2016]. The appropriate choice, particularly for large-scale regional simulations, is dependent on whether the necessary input data exist and whether the model is run at sufficient spatial resolution to implement more sophisticated model physics. For example, Radić *et al.* [2013] note that ice thickness data, required for a physically based ice flow model, are available for less than 1% of the glaciers in the world. Huss and Farinotti [2012] help to fill this data gap by providing estimates of spatially distributed glacier thickness globally (using RGI areal extent, DEMs, highly parametrized surface mass balances, and an inverse model for the thickness), but these estimates come with considerable uncertainties. An approach of intermediate complexity [Huss *et al.*, 2010] may therefore be best suited in the near future.

In section 4.4, we argue that the  $AAR_0$  case is preferred over the transient AAR case since it produces future glacier runoff values that are consistent with Bliss *et al.* [2014]. Calculations of the water storage in the study domain also support this choice. Beamer *et al.* [2016] noted that an analysis of GRACE data for the GOA domain show a trend of  $-60.1 \text{ km}^3 \text{ yr}^{-1}$  and that this agreed very well with water balance calculations from the CFSR-forced model runs ( $-60 \text{ km}^3 \text{ yr}^{-1}$ ). In the present study, the future (2070–2099) trends based on the  $AAR_0$  assumption are  $-74 \text{ km}^3 \text{ yr}^{-1}$  for the RCP 4.5 case and  $-62 \text{ km}^3 \text{ yr}^{-1}$  for the RCP 8.5 case. For the transient AAR simulations, the corresponding trends are  $-147$  and  $-170 \text{ km}^3 \text{ yr}^{-1}$ . Given that the projections of warming described in section 4.2.1 are comparable to the historic observations of warming described by Bieniek *et al.* [2014] and Arendt *et al.* [2009], it is reasonable to expect future trends to be comparable to recent trends rather than 2.5–3 times greater. Therefore, we conclude (Table 2) that future GOA runoff will increase from  $760 \text{ km}^3 \text{ yr}^{-1}$  (historic) to  $830 \text{ km}^3 \text{ yr}^{-1}$  under the RCP4.5 scenario and  $865 \text{ km}^3 \text{ yr}^{-1}$  under the RCP8.5 scenario for the 2070–2099 climatological periods. Runoff from glacier surfaces will decrease from  $290 \text{ km}^3 \text{ yr}^{-1}$  (historic) to  $250$  and  $190 \text{ km}^3 \text{ yr}^{-1}$ , respectively, for that period.

Although our hypsographic model is informed by ELA and AAR values derived from process-based studies [Huss and Hock, 2015], it is clearly a first-order approach to determining likely future glacier cover. It is fully decoupled from and only provides an input (glacier cover) to the hydrologic modeling. Additionally, it ignores processes related to tidewater glaciers. From a hydrological perspective, by not evolving the glacier extent (i.e., retreat) during the 30 year run the glacier runoff estimates are probably overestimated, but by not evolving the glacier elevations (i.e., thinning) it is underestimated. In addition, using the steady state  $AAR_0$  value, instead of a transient (typically decreasing) [Huss and Hock, 2015] AAR value, retains less ice at

lower elevations and may result in an underestimate of glacier runoff. These opposing biases may partially offset each other, reducing the overall bias in modeled glacier runoff, although that is not rigorously investigated in this study.

### 5.3. Implications of Changes

ROS events, while likely having limited impact on the snowpack energy balance [Mazurkiewicz et al., 2008], can nevertheless fundamentally alter the physical characteristics of snowpacks. Rain can rapidly densify snow [Marshall et al., 1999] leading to slope instabilities and avalanching [Conway and Raymond, 1993] and can increase the speed of water transfer through the snowpack [Singh et al., 1997]. We find ROS accounts for approximately 20% of snowpack runoff in our historical simulations, suggesting ROS events already play an important role in affecting snowpack physics in the GOA region.

Our future simulations show that the majority of wintertime increases in snowpack runoff are due to ROS events, rather than increases in snowpack melting. Therefore, even though surface temperature increases may be insufficient to drive significant melt events during the winter, atmospheric temperature increases cause more precipitation to fall as rain instead of snow. This provides a potential positive feedback mechanism whereby snowpack densification, decreases in surface albedo, and the formation of superimposed ice layers can enhance melt and runoff during the arrival of the next summer melt season.

Our study assesses the regional consequences of major reductions in the two major water storage reservoirs (seasonal snowpack and glaciers) in the GOA. Water from these reservoirs is currently and historically released in the spring and into the summer, and this slow release provides a stable water supply in the drier summer months. Low-elevation snowpack provides moisture for soils, and snowmelt is more efficient than rainfall at recharging groundwater aquifers. In our climate change simulations forced by the greatest atmospheric warming (RCP 8.5), the peak SWE volume in the GOA decreases by 31% from  $\sim 360 \text{ km}^3$  to  $\sim 250 \text{ km}^3$ , with widespread reduction in the snow covered area and particularly large losses at low elevations. The glacier covered area in the ELA 400 AAR<sub>0</sub> case is reduced by 34%. The reduction in SWE cover and volume reduces available snowpack for spring runoff and groundwater recharge, diminishes mass input to replenish glaciers, and decreases the spring snow extent for low to mid elevations.

A major new source for runoff appears in the autumn and winter months due to the pronounced shift from snow to rain driven by atmospheric warming and increased precipitation amounts (increased magnitude). Rainfall runs off immediately, resulting in flashier hydrographs compared to the steadier and more stable hydrographs associated with spring snowmelt and glacier ice melt. Since the rainfall runoff tracks more closely with the precipitation patterns, there is a higher likelihood of low summer flows, and therefore reduced groundwater recharge and drier soils during these months.

## 6. Conclusions

We used a suite of high-resolution regional-scale hydrologic models to quantify the response of late 21st century runoff from the GOA to temperature and precipitation changes from five GCMs and two emission scenarios, along with future glacier extents derived from predicted ELA increases. Pronounced atmospheric warming of 2.5–4.3°C was evident for all seasons and all regions of the GOA, a robust finding across all GCMs and emission scenarios. Annual precipitation inputs to the GOA also increased for all GCMs and emission scenarios. As a result of these climate perturbations, both the percentage of precipitation that fell as snow and the peak snowpack volume decreased, resulting in reduced snow cover extent and subsequent runoff generated by snowmelt. Our hypsographic modeling resulted in a steep decline in areal extent of glaciers within the GOA watershed that was particularly sensitive (decrease ranged between –15% and –57%) to the selection of the representative AAR value, highlighting the importance of accurately modeling future glacier cover. To improve this prediction, both improvements in model input data (observations of key glacier parameters, such as ice thickness and snow accumulation spatial variability) and model sophistication (i.e., incorporation of ice dynamics) are required.

Using the projected climate data and altered glacier cover, model runs were made to determine the change in terrestrial and glacier runoff from the period 1980–2009 to the period 2070–2099. Glacier runoff estimates and regional water storage calculations supported the use of AAR<sub>0</sub>. With this AAR<sub>0</sub>, total annual runoff to the GOA increases by 9% and 14% for the RCP 4.5 and RCP 8.5 scenarios. There are large relative

increases in rainfall runoff during winter months due to increasing precipitation and decreasing snow-rain fraction. In the summer months, there are decreases in runoff due to less snow and ice melt. Glacier runoff (runoff from glacier surfaces) decreases to 86% and 66% of the historical value for the 4.5 and 8.5 scenarios. On a watershed-by-watershed basis, responses were variable depending upon watershed elevation and initial land cover characteristics (substantially glaciated or not). We anticipate that future studies of runoff modeling in spatially complex, regional-scale, coastal mountain environments will benefit primarily from improvements to model processes (glacier evolution) rather than model inputs.

## Appendix

The table below provides values for many of the model parameters used in this study. In some cases, the parameter values were selected from the calibration described in Beamer *et al.* [2016]. In other cases, commonly used default values were used.

### Acknowledgments

The authors acknowledge the North Pacific Research Board Graduate Research Fellowship program (NPRB publication no. 605), the Oil Spill Recovery Institute (grant 12-10-07), NASA Cryospheric Sciences program (grant NNX16AF14G), the Washington Research Foundation Fund for Innovation in Data-Intensive Discovery, the Moore/Sloan Data Science Environments Project at the University of Washington, USGS Alaska Climate Science Center Ice2O: Assessing Icefield-to-Ocean Change in the Pacific Coastal Temperate Rainforest project, USGS Climate and Land Use Change program, and the CUAHSI Pathfinder Fellowship Program for funding components of this effort. We also thank Glen Liston from Colorado State University for his generosity in providing the model code. Any use of trade, firm, or product names is for descriptive purposes only and does not imply endorsement by the U.S. Government. The data used for this project are available as follows: (i) Digital elevation model <https://lta.cr.usgs.gov/HYDRO1K>; (ii) Land cover—<http://www.cec.org/tools-and-resources/map-files/land-cover-2005>; (iii) Randolph Glacier Inventory—[http://www.glims.org/RGI/rgi32\\_dl.html](http://www.glims.org/RGI/rgi32_dl.html); (iv) Soils data—<http://www.fao.org/soils-portal/soil-survey/soil-maps-and-databases/harmonized-world-soil-database-v12/en/>; (v) CFSR data—<http://rda.ucar.edu/datasets/ds093.0/>; (vi) SNAP data—<http://ckan.snap.raf.edu/dataset>; (vii) NHD data—<http://nhd.usgs.gov/data.html>; and (viii) Transboundary drainage areas—<http://gis.jic.org/arcgis/rest/services/Base-Data/TransboundaryDrainageAreas/MapServer>. Model output included daily time series of numerous variables. These variables were aggregated spatially across the Gulf of Alaska watershed and temporally over a 30 year (2070–2099) period. The climatologies of model inputs and outputs that served as the basis of the figures in this paper can be accessed in the supporting information (SI) file.

Variable	Parameter Name	Value	Citation
n	Number of nearest stations used for interpolation	5	Daly <i>et al.</i> [2002]
L	Curvature length scale (m) used for wind model	500	Liston [1995]
ws <sub>min</sub>	Minimum wind speed ( $m s^{-1}$ )	1.0	Liston and Elder [2006a, 2006b]
$\Gamma$	Monthly temperature lapse rate ( $^{\circ}C km^{-1}$ )	2.4–5.6	Beamer <i>et al.</i> [2016]
$\chi$	Monthly precipitation adjustment factor ( $km^{-1}$ )	0.2–0.35	Beamer <i>et al.</i> [2016]
T <sub>snow/rain</sub>	Snow/rain threshold temperatures ( $^{\circ}C$ )	0.0/2.0	Fuchs <i>et al.</i> [2001]
g	Canopy gap fraction	0.2	Liston and Elder [2006a, 2006b]
$\alpha_s$ , fresh	Fresh nonmelting snow albedo	0.80	Mernild <i>et al.</i> [2008]
$\alpha_s$ , melt-forest	Melting snow albedo, under forest canopy	0.45	Liston and Elder [2006a, 2006b]
$\alpha_s$ , melt-clearing	Melting snow albedo, nonforested area	0.60	Liston and Elder [2006a, 2006b]
$\alpha_{ice}$	Bare glacier albedo, dry and melting	0.30	Beamer <i>et al.</i> [2016]
$\alpha_s$ , forest	Forest vegetation albedo	0.15	McMahon <i>et al.</i> [2013]
$\alpha_s$ , shrub/grass	Grassland vegetation albedo	0.25	McMahon <i>et al.</i> [2013]
$\alpha_s$ , water	Open water albedo	0.08	McMahon <i>et al.</i> [2013]
$\rho_{snow}$	Initial snow density ( $kg m^{-3}$ )	300	Liston [1995]
	Zero snow date (for multiyear simulations)	1 Sep	Beamer <i>et al.</i> [2016]
$\alpha_{PT}$	Priestley-Taylor coefficient	1.26	McMahon <i>et al.</i> [2013]
$k_b$	Base flow coefficient ( $mm d^{-1}$ )	0.1	Beamer <i>et al.</i> [2016]
V <sub>ice, sc</sub>	Flow velocity ( $m s^{-1}$ ) through snow-covered ice	0.12	Liston and Mernild [2012]
V <sub>ice, sf</sub>	Flow velocity ( $m s^{-1}$ ) through snow-free ice	0.20	Liston and Mernild [2012]
V <sub>land, sc</sub>	Flow velocity ( $m s^{-1}$ ) through snow-covered land	0.10	Liston and Mernild [2012]
V <sub>land, sf</sub>	Flow velocity ( $m s^{-1}$ ) through snow-free land	0.08	Liston and Mernild [2012]
$\alpha_{slow}$	Slow flow velocity scaling parameter	20	Beamer <i>et al.</i> [2016]
$\alpha_{fast}$	Fast flow velocity scaling parameter	3	Beamer <i>et al.</i> [2016]

## References

- Arendt, A., J. Walsh, and W. Harrison (2009), Changes of glaciers and climate in northwestern North America during the late twentieth century, *J. Clim.*, 22, 4117–4134, doi:10.1175/2009JCLI2784.1.
- Bavay, M., T. Grunewald, and M. Lehning (2013), Response of snow cover and runoff to climate change in high Alpine catchments of Eastern Switzerland, *Adv. Water Resour.*, 55, 4–16, doi:10.1016/j.advwatres.2012.12.009.
- Beamer, J. P., D. F. Hill, A. Arendt, and G. E. Liston (2016), High-resolution modeling of coastal freshwater discharge and glacier mass balance in the Gulf of Alaska watershed, *Water Resour. Res.*, 52, 3888–3909, doi:10.1002/2015WR018457.
- Bieniek, P. A., J. E. Walsh, R. L. Thoman, and U. S. Bhatt (2014), Using climate divisions to analyze variations and trends in Alaska temperature and precipitation, *J. Clim.*, 27, 2800–2818, doi:10.1175/JCLI-D-13-00342.1.
- Bieniek, P. A., et al. (2015a), Climate drivers linked to changing seasonality of Alaska Coastal Tundra vegetation productivity, *Earth Interact.*, 19, 1–29, doi:10.1175/El-D-15-0013.1.
- Bieniek, P. A., U. S. Bhatt, J. E. Walsh, T. S. Rupp, J. Zhang, J. R. Krieger, and R. Lader (2015b), Dynamical downscaling of ERA-Interim temperature and precipitation for Alaska, *J. Appl. Meteorol. Climatol.*, 55, 635–654, doi:10.1175/JAMC-D-15-0153.1.
- Bliss, A., R. Hock, and V. Radic (2014), Global response of glacier runoff to twenty-first century climate change, *J. Geophys. Res. Earth Surf.*, 119, 717–730, doi:10.1002/2013JF002931.
- Clarke, G. K. C., A. H. Jarosch, F. S. Anslow, V. Radic, and B. Menounos (2015), Projected deglaciation of western Canada in the twenty-first century, *Nat. Geosci.*, 8, 372–377, doi:10.1038/ngeo2407.
- Conway, H., and C. F. Raymond (1993), Snow stability during rain, *J. Glaciol.*, 39(133), 635–642, doi:10.3198/1993JoG39-133-635-642.
- Daly, C., W. P. Gibson, G. H. Taylor, G. L. Johnson, and P. Pasteris (2002), A knowledge-based approach to the statistical mapping of climate, *Clim. Res.*, 22(2), 99–113, doi:10.3354/cr022099.
- Engelhardt, M., T. V. Schuler, and L. M. Andreassen (2015), Sensitivities of glacier mass balance and runoff to climate perturbations in Norway, *Ann. Glaciol.*, 56, 79–88, doi:10.3189/2015AoG70A004.

- Fellman, J. B., R. G. M. Spencer, P. J. Hernes, R. T. Edwards, D. V. D'Amore, and E. Hood (2010), The impact of glacier runoff on the biodegradability and biochemical composition of terrigenous dissolved organic matter in near-shore marine ecosystems, *Mar. Chem.*, 121(1–4), 112–122, doi:10.1016/j.marchem.2010.03.009.
- Fischer, G., F. O. Nachtergaele, S. Pryler, H. van Velthuizen, L. Verelst, and D. Wiberg (2008), *Global Agro-Ecological Zones Assessment for Agriculture (GAEZ 2008)*, IIASA, Laxenburg, Austria.
- Flint, L. E., A. L. Flint, J. H. Thorne, and R. Boynton (2013), Fine-scale hydrologic modeling for regional landscape applications: The California Basin Characterization Model development and performance, *Ecol. Process.*, 2, 25, doi:10.1186/2192-1709-2-25.
- Fowler, H., S. Bleikinsop, and C. Tebaldi (2007), Review—Linking climate change modeling to impacts studies: Recent advances in downscaling techniques for hydrological modeling, *Int. J. Climatol.*, 27, 1547–1578.
- Fuchs, T., J. Rapp, F. Rubel, and B. Rudolf (2001), Correction of synoptic precipitation observations due to systematic measuring errors with special regard to precipitation phases, *Phys. Chem. Earth, Part B*, 26(9), 689–693, doi:10.1016/S1464-1909(01)00070-3.
- Hickey, B. M., and N. S. Banas (2003), Oceanography of the U.S. Pacific Northwest Coastal Ocean and estuaries with application to coastal ecology, *Estuaries*, 26, 1010–1031, doi:10.1007/BF02803360.
- Hill, D. F., N. Bruhis, S. E. Calos, A. Arendt, and J. Beamer (2015), Spatial and temporal variability of freshwater discharge into the Gulf of Alaska, *J. Geophys. Res. Oceans*, 120, 634–646, doi:10.1002/2014JC010395.
- Hodgkins, G. A. (2009), Streamflow changes in Alaska between the cool phase (1947–1976) and the warm phase (1977–2006) of the Pacific Decadal Oscillation: The influence of glaciers, *Water Resour. Res.*, 45, W06502, doi:10.1029/2008WR007575.
- Huss, M., and D. Farinotti (2012), Distributed ice thickness and volume of all glaciers around the globe, *J. Geophys. Res.*, 117, F04010, doi:10.1029/2012JF002523.
- Huss, M., and R. Hock (2015), A new model for global glacier change and sea-level rise, *Cryospheric Sci.*, 54, 1–22, doi:10.3389/fcse.2015.00054.
- Huss, M., G. Jouvet, D. Farinotti, and A. Bauder (2010), Future high-mountain hydrology: A new parameterization of glacier retreat, *Hydro. Earth Syst. Sci.*, 14, 815–829, doi:10.5194/hess-14-815-2010.
- Huss, M., M. Zemp, P. C. Joerg, and N. Salzmann (2014), High uncertainty in 21st century runoff projections from glacierized basins, *J. Hydrol.*, 510, 35–48, doi:10.1016/j.jhydrol.2013.12.017.
- Immerzeel, W. W., L. P. H. van Beek, M. Konz, A. B. Shrestha, and M. F. P. Bierkens (2012), Hydrological response to climate change in a glacierized catchment in the Himalayas, *Clim. Change*, 110, 721–736, doi:10.1007/s10584-011-0143-4.
- Kienholz, C., S. Herreid, J. L. Rich, A. A. Arendt, R. Hock, and E. W. Burgess (2015), Derivation and analysis of a complete modern-date glacier inventory for Alaska and northwest Canada, *J. Glaciol.*, 61, 403–420, doi:10.3189/2015JoG14J230.
- Knutti, R., and J. Sedláček (2013), Robustness and uncertainties in the new CMIP5 climate model projections, *Nat. Clim. Change*, 3, 369–373, doi:10.1038/nclimate1716.
- Kustas, W. P., A. Rango, and R. Uijlenhoet (1994), A simple energy budget algorithm for the snowmelt runoff model, *Water Resour. Res.*, 30, 1515–1527, doi:10.1029/94WR00152.
- Lader, R., U. S. Bhatt, J. E. Walsh, T. S. Rupp, and P. A. Bieniek (2016), Two-meter temperature and precipitation from atmospheric reanalysis evaluated for Alaska, *J. Appl. Meteorol. Climatol.*, 55, 901–922, doi:10.1175/JAMC-D-15-0162.1.
- Larsen, C. F., E. Burgess, A. A. Arendt, S. O'Neal, A. J. Johnson, and C. Kienholz (2015), Surface melt dominates Alaska glacier mass balance, *Geophys. Res. Lett.*, 42, 5902–5908, doi:10.1002/2015GL064349.
- Liang, X., D. P. Lettenmaier, E. F. Wood, and S. J. Burges (1994), A simple hydrologically based model of land surface water and energy fluxes for general circulation models, *J. Geophys. Res.*, 99, 14,415–14,428, doi:10.1029/94JD00483.
- Liston, G. E. (1995), Local advection of momentum, heat, and moisture during the melt of patchy snow covers, *J. Appl. Meteorol.*, 34(7), 1705–1715, doi:10.1175/1520-0450-34.7.1705.
- Liston, G. E., and K. Elder (2006a), A meteorological distribution system for high-resolution terrestrial modeling (MicroMet), *J. Hydrometeorol.*, 7, 217–234, doi:10.1175/JHM486.1.
- Liston, G. E., and K. Elder (2006b), A distributed snow-evolution modeling system (SnowModel), *J. Hydrometeorol.*, 7, 1259–1276, doi:10.1175/JHM548.1.
- Liston, G. E., and S. H. Mernild (2012), Greenland freshwater runoff. Part I: A runoff routing model for glaciated and nonglaciated landscapes (HydroFlow), *J. Clim.*, 25, 5997–6014, doi:10.1175/JCLI-D-11-00591.1.
- Mantua, N. J., S. R. Hare, Y. Zhang, J. M. Wallace, and R. C. Francis (1997), A Pacific interdecadal climate oscillation with impacts on salmon production, *Bull. Am. Meteorol. Soc.*, 78, 1069–1079, doi:10.1175/1520-0477(1997)078<1069:APICOW>2.0.CO;2.
- Marshall, H. P., H. Conway, and L. A. Rasmussen (1999), Snow densification during rain, *Cold Reg. Sci. Technol.*, 30(1–3), 35–41, doi:10.1016/S0165-232X(99)00011-7.
- Mazurkiewicz, A. B., D. G. Callery, and J. J. McDonnell (2008), Assessing the controls of the snow energy balance and water available for runoff in a rain-on-snow environment, *J. Hydrol.*, 354(1–4), 1–14, doi:10.1016/j.jhydrol.2007.12.027.
- McAfee, S. A., J. Walsh, and T. S. Rupp (2014), Statistically downscaled projections of snow/rain partitioning for Alaska, *Hydro. Processes*, 28, 3930–3946, doi:10.1002/hyp.9934.
- McGrath, D., L. Sass, S. O'Neal, A. Arendt, and C. Kienholz (2017), Hypsometric control on glacier mass balance sensitivity in Alaska and Northwest Canada, *Earth's Future*, 5, 324–336, doi:10.1002/2016EF000479.
- McMahon, T. A., M. C. Peel, L. Lowe, R. Srikanthan, and T. R. McVicar (2013), Estimating actual, potential, reference crop and pan evaporation using standard meteorological data: A pragmatic synthesis, *Hydro. Earth Syst. Sci.*, 17(4), 1331–1363, doi:10.5194/hess-17-1331-2013.
- Mernild, S. H., G. E. Liston, C. A. Hiemstra, and K. Steffen (2008), Surface melt area and water balance modeling on the Greenland Ice Sheet 1995–2005, *J. Hydrometeorol.*, 9(6), 1191–1211, doi:10.1175/2008JHM957.1.
- Mernild, S. H., W. H. Lipscomb, D. B. Bahr, V. Radić, and M. Zemp (2013), Global glacier changes: A revised assessment of committed mass losses and sampling uncertainties, *Cryosphere*, 7, 1565–1577, doi:10.5194/tc-7-1565-2013.
- Mosier, T. M., D. F. Hill, and K. V. Sharp (2016), How much cryosphere model complexity is just right? Exploration using the conceptual cryosphere hydrology framework, *Cryosphere*, 10, 2147–2171, doi:10.5194/tc-10-2147-2016.
- Mpelasoka, F., and F. Chiew (2009), Influence of rainfall scenario construction methods on runoff projections, *J. Hydrometeorol.*, 10, 1168–1183.
- Neal, E. G., E. Hood, and K. Smikrud (2010), Contribution of glacier runoff to freshwater discharge into the Gulf of Alaska, *Geophys. Res. Lett.*, 37, L06404, doi:10.1029/2010GL042385.
- O'Neal, S., et al. (2015), Icefield-to-ocean linkages across the Northern Pacific coastal temperate rainforest ecosystem, *BioScience*, 65, 499–512, doi:10.1093/biosci/biv027.
- Paul, F., M. Maisch, C. Rothenbühler, M. Hoelzle, and W. Haeberli (2007), Calculation and visualisation of future glacier extent in the Swiss Alps by means of hypsographic modelling, *Global Planet. Change*, 55, 343–357, doi:10.1016/j.gloplacha.2006.08.003.

- Pfeffer, W. T., et al. (2014), The Randolph Glacier Inventory: A globally complete inventory of glaciers, *J. Glaciol.*, 60, 537–552, doi:10.3189/2014JG13J176.
- Priestley, C. H. B., and R. J. Taylor (1972), On the assessment of surface heat flux and evaporation using large-scale parameters, *Mon. Weather Rev.*, 100, 81–92, doi:10.1175/1520-0493(1972)100<0081:OTAOSH>2.3.CO;2.
- Radić, V., and R. Hock (2006), Modeling future glacier mass balance and volume changes using ERA-40 reanalysis and climate models: A sensitivity study at Storglaciären, Sweden, *J. Geophys. Res.*, 111, F03003, doi:10.1029/2005JF000440.
- Radić, V., A. Bliss, A. C. Beedlow, R. Hock, E. Miles, and J. G. Cogley (2013), Regional and global projections of twenty-first century glacier mass changes in response to climate scenarios from global climate models, *Clim. Dyn.*, 42, 37–58, doi:10.1007/s00382-013-1719-7.
- Reisdorph, S. C., and J. T. Mathis (2014), The dynamic controls on carbonate mineral saturation states and ocean acidification in a glacially dominated estuary, *Estuarine Coastal Shelf Sci.*, 144, 8–18, doi:10.1016/j.ecss.2014.03.018.
- Royer, T. C., and C. E. Grosch (2006), Ocean warming and freshening in the northern Gulf of Alaska, *Geophys. Res. Lett.*, 33, L16605, doi:10.1029/2006GL026767.
- Saha, S., et al. (2010), The NCEP Climate Forecast System Reanalysis, *Bull. Am. Meteorol. Soc.*, 91, 1015–1057, doi:10.1175/2010BAMS3001.1.
- Schaeffli, B., B. Hingray, M. Niggli, and A. Musy (2005), A conceptual glacio-hydrological model for high mountainous catchments, *Hydrolog. Earth Syst. Sci.*, 9, 95–109, doi:10.5194/hess-9-95-2005.
- Schnorbus, M., A. Werner, and K. Bennett (2014), Impacts of climate change in three hydrologic regimes in British Columbia, Canada, *Hydrolog. Processes*, 28, 1170–1189, doi:10.1002/hyp.9661.
- Shanley, C. S., and D. M. Albert (2014), Climate change sensitivity index for Pacific salmon habitat in Southeast Alaska, *PLoS ONE*, 9, e104799, doi:10.1371/journal.pone.0104799.
- Shrestha, R. R., M. A. Schnorbus, A. T. Werner, and F. W. Zwiers (2013), Evaluating Hydroclimatic change signals from statistically and dynamically downscaled GCMs and hydrologic models, *J. Hydrometeorol.*, 15, 844–860, doi:10.1175/JHM-D-13-030.1.
- Singh, P., G. Spitzbart, H. Hübl, and H. W. Weinmeister (1997), Hydrological response of snowpack under rain-on-snow events: A field study, *J. Hydrol.*, 202(1–4), 1–20, doi:10.1016/S0022-1694(97)00004-8.
- Sulis, M., C. Paniconi, M. Marrocù, D. Huard, and D. Chaumont (2012), Hydrologic response to multimodel climate output using a physically based model of groundwater/surface water interactions, *Water Resour. Res.*, 48, W12510, doi:10.1029/2012WR012304.
- Walsh, J. E., W. L. Chapman, V. Romanovsky, J. H. Christensen, and M. Stendel (2008), Global climate model performance over Alaska and Greenland, *J. Clim.*, 21, 6156–6174, doi:10.1175/2008JCLI2163.1.
- Wobus, C., R. Prucha, D. Albert, C. Woll, M. Loinaz, and R. Jones (2015), Hydrologic alterations from climate change inform assessment of ecological risk to Pacific Salmon in Bristol Bay, Alaska, *PLoS ONE*, 10, e0143905, doi:10.1371/journal.pone.0143905.
- Ziemer, F. A., R. Hock, A. Aschwanden, C. Khroulev, C. Kienholz, A. Melkonian, and J. Zhang (2016), Modeling the evolution of the Juneau Icefield between 1971 and 2100 using the Parallel Ice Sheet Model (PISM), *J. Glaciol.*, 62, 199–214, doi:10.1017/jog.2016.13.